LETTERS
PUBLISHED ONLINE: 12 JUNE 2011 | DOI: 10.1038/NPHOTON.2011.99
nature photonics

Single-cell biological lasers

Malte C. Gather[1,2] and Seok Hyun Yun[1,2,3,4]*

Since their invention some 50 years ago[1], lasers have made a tremendous impact on modern science and technology. Nevertheless, lasing has so far relied on artificial or engineered optical gain materials, such as doped crystals, semiconductors, synthetic dyes and purified gases[2,3]. Here, we show that fluorescent proteins[4,5] in cells are a viable gain medium for optical amplification, and report the first successful realization of biological cell lasers based on green fluorescent protein (GFP). We demonstrate *in vitro* protein lasers using recombinant GFP solutions and introduce a laser based on single live cells expressing GFP. On optical pumping with nanojoule/nanosecond pulses, individual cells in a high-Q microcavity produce bright, directional and narrowband laser emission, with characteristic longitudinal and transverse modes. Lasing cells remained alive even after prolonged lasing action. Light amplification and lasing from and within biological systems pave the way to new forms of intracellular sensing, cytometry and imaging.

Green fluorescent protein (GFP), first purified from the jellyfish *A. victoria*[6], has become an indispensible tool in biomedical science as a reporter protein and imaging tracer. GFP can be expressed as a functional transgene in a wide variety of organisms[7] and thus enables monitoring of gene expression, tracking of GFP-fusion proteins in cells *in vitro* and visualization of GFP-expressing cells *in vivo* in animal models. Directed mutation of GFP and other fluorescent proteins from different organisms has yielded variants with improved maturation, brightness and stability[8,9], as well as emission bands across the entire visible spectrum[10,11]. Because of the excellent optical properties of these proteins, including transition cross-sections higher than 2×10^{-16} cm^2 and near 80% fluorescence quantum yields[12], they are promising gain media for stimulated emission and biolasing. In fact, some evidence that GFP can support lasing with two-photon excitation has been reported[13].

When pumped at an appropriate wavelength, fluorescent proteins are expected to form a quasi-four-level laser system[14]. Following absorption of a pump photon, the protein undergoes a transition from the ground-state S_0 to a higher electronic state S_1 (Fig. 1a). Both states are composed of a quasi-continuum of vibrational sublevels giving rise to broad optical absorption and emission spectra. The absorption is followed by rapid non-radiative relaxation to the metastable lowest vibrational state of the S_1 manifold, from which stimulated emission to different vibrational states of S_0 can occur. Because the lifetime of S_1 is typically a few nanoseconds, population inversion between the lowest vibrational state of S_1 and the vibrational sublevels of S_0—a necessary condition for net gain—can be achieved most conveniently by optical pumping with nanosecond or shorter pulses.

To characterize GFP as a gain material, we first investigated aqueous solutions of purified GFP harvested from bacterial culture (recombinant GFP). We constructed a simple low-loss optical resonator consisting of two concave mirrors (interspacing, $d = 7$ mm; curvatures, 10 mm and 50 mm; see Methods). Both mirrors had a dichroic coating with high reflectivity ($R > 99.5\%$) in a wavelength (λ) range between 500 and 560 nm and high transmission at $\lambda < 480$ nm. To avoid unnecessary reflection losses, the cavity space between the mirrors was completely filled with an aqueous 50 μM solution of recombinant eGFP, a widely used mutant of the wild-type GFP. The solution was pumped longitudinally by focusing the output pulses from an optical parametric oscillator (OPO: $\lambda = 465$ nm; duration, 5 ns; repetition rate, 10 Hz) into the cavity (Fig. 1b).

Figure 1c shows the amount of light emitted through the cavity mirror (output energy) as a function of the pump energy E_p (per pulse). Above a threshold E_p of 14 nJ, the output energy rose dramatically faster with increasing pump energy than at smaller E_p and bright green light was emitted that was clearly visible with the naked eye. The emission spectrum was substantially narrowed (FWHM, 12 nm) compared to the free-space spontaneous fluorescence spectrum (FHWM, 37 nm) of the eGFP solution (Fig. 1d) and the subthreshold emission spectrum of the resonator (Fig. 1e). The presence of a sharp threshold above which the cavity output rapidly increases and spectral narrowing occurs is clear evidence of lasing and demonstrates that eGFP can provide significant optical gain. The 12 nm linewidth indicates simultaneous oscillation of numerous longitudinal modes in the relatively long cavity. The laser wavelength was independent of the excitation wavelength (Supplementary Fig. S1), which rules out stimulated scattering processes as an alternative explanation for our observations. The spatial profile of the laser output corresponded to the typical fundamental transverse electromagnetic mode, TEM_{00} (Fig. 1f(i)). Following deliberate misalignment of the cavity (by slightly tilting one mirror), the spatial profile changed to patterns indicating operation at higher-order TEM modes (Fig. 1f(ii–iv)). Even when operated at $E_p = 2.5$ μJ (that is, ~200 times the threshold), no noticeable sign of reduction in the output energy was observed over the course of 5,000 pump pulses (500 s).

We observed lasing with eGFP concentrations as small as 2.5 μM. As the concentration was reduced, the lasing wavelength shifted towards the blue (Fig. 1d). This is expected, as self-absorption from the tail of the eGFP absorption band is less significant at low concentrations. At concentrations higher than 100 μM, the threshold pump energy increased with concentration as absorption by unexcited eGFP began to contribute significantly to the overall cavity loss (Fig. 1g). Typical GFP concentrations in the cytosol of biological cells range from micromolar to millimolar[15,16]. Therefore, we have reasoned that it should be possible to achieve lasing with a single GFP-expressing cell if a resonator with sufficiently low loss is used.

To realize a cell laser, we transiently transfected mammalian cells (293ETN cells[17] derived from the human embryonic kidney cell line

[1]Wellman Center for Photomedicine, Massachusetts General Hospital, 55 Fruit Street, Boston, Massachusetts 02114, USA, [2]Department of Dermatology, Harvard Medical School, 55 Fruit Street, Boston, Massachusetts 02114, USA, [3]WCU Graduate School of Nanoscience and Technology, Korea Advanced Institute of Science and Technology, Daejeon, Korea, [4]Harvard–MIT Health Sciences and Technology, Cambridge, Massachusetts, USA.
*e-mail: syun@hms.harvard.edu

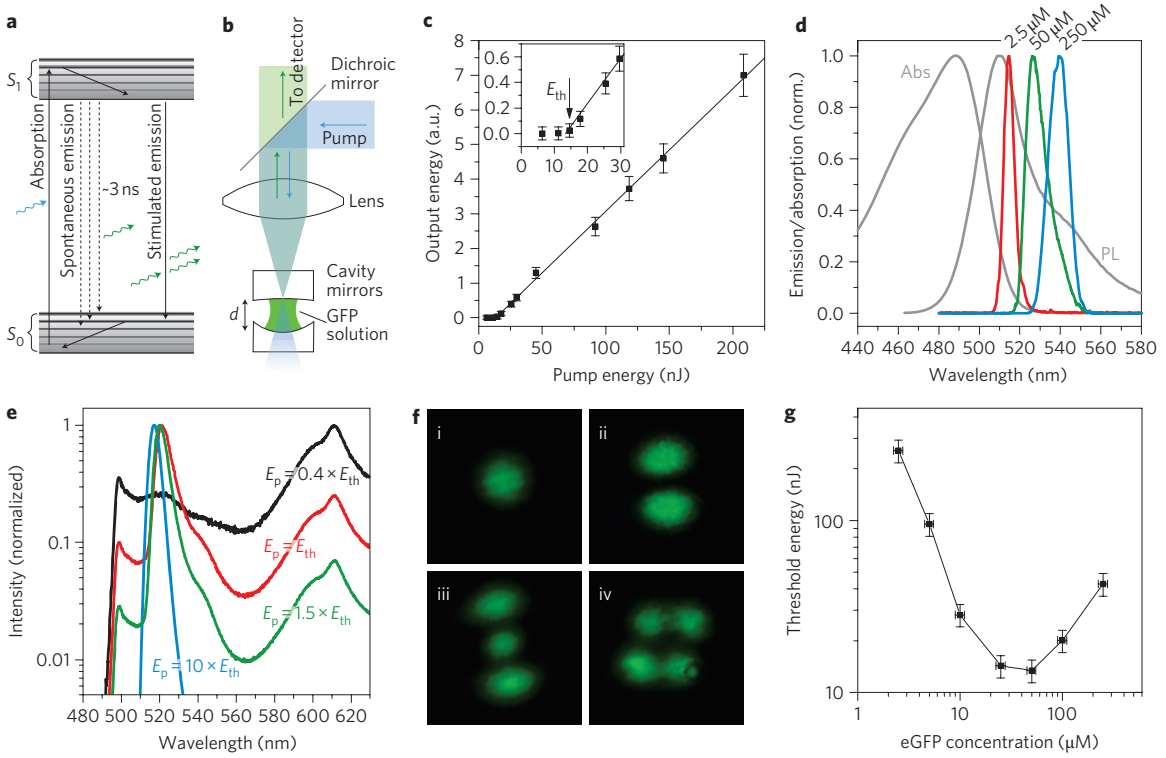

Figure 1 | A protein solution laser. a, Energy diagram of the quasi-four-level laser system eGFP with relevant transitions: absorption, vibrational relaxation, stimulated emission and vibrational relaxation. **b**, Schematic of the protein solution laser. Pump light is reflected by a dichroic mirror and focused into the GFP-filled cavity by a lens that also collects the cavity emission ($d = 7$ mm). **c**, Laser output energy as a function of pump energy E_p (symbols). Line is a linear fit to data above 14 nJ. Error bars represent detector noise and pulse-to-pulse variation. Inset, close-up on data around the lasing threshold E_{th}. **d**, Spontaneous photoluminescence spectrum (PL) and normalized absorption spectrum (Abs) of a 10 μM eGFP solution. Normalized output spectra of the laser filled with eGFP solutions with concentrations of 2.5, 50 and 250 μM ($E_p = 5 \times E_{th}$). **e**, Normalized laser spectra at different pump energies (eGFP concentration, 5 μM). As the transmission of the cavity mirror is strongly wavelength-dependent, the subthreshold spectrum (black) differs substantially from the PL spectrum in **d**. **f**, Beam profiles of the laser emission in optimal (i) and misaligned conditions (ii–iv), corresponding to the TEM_{00}, TEM_{01}, TEM_{02} and TEM_{11} transverse modes. **g**, Measured lasing threshold for different concentrations of eGFP (symbols). Error bars represent uncertainty in the linear fit to input-output characteristic (y) and in concentration of the respective solutions (x).

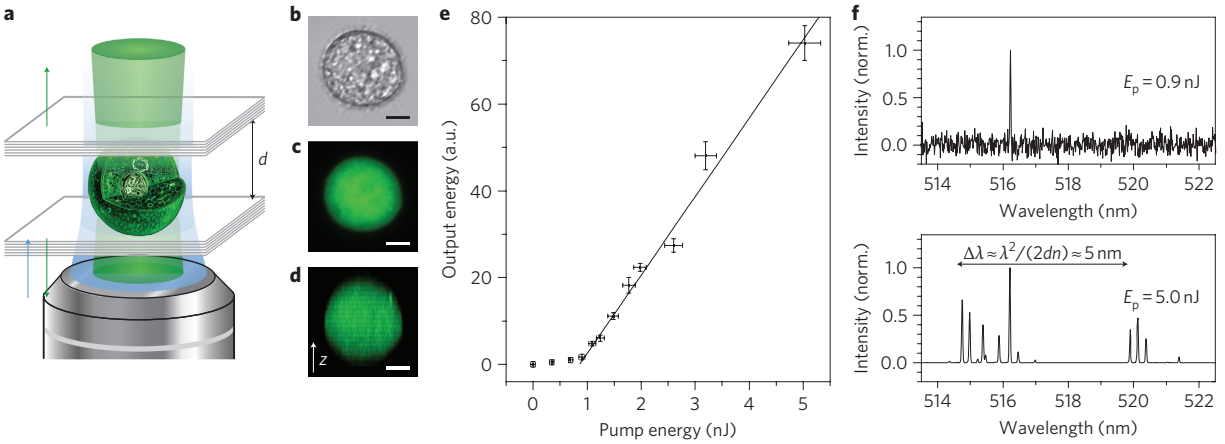

Figure 2 | Laser formed by a single eukaryotic cell. a, Illustration of the single-cell laser. A live eGFP-expressing 293ETN cell is placed inside a high-Q resonator consisting of two DBRs ($d = 20$ μm). **b**–**d**, Microscope images of a single 293ETN cell outside the resonator (scale bars, 5 μm): DIC image (**b**); confocal fluorescence microscope image showing the eGFP distribution in the cell (**c**); side-view projection of a z-stack of confocal fluorescence images (**d**). **e**, Laser output energy of a cell laser as a function of the pump energy. Line, linear fit to data above 1 nJ. Error bars represent detector noise and pulse-to-pulse variation of output (y), and pulse-to-pulse variation of pump (x), respectively. **f**, Normalized output spectra of the same laser for pump energies of 0.9 and 5 nJ, respectively. The arrow denotes the expected wavelength spacing of consecutive longitudinal modes.

HEK293) with a plasmid encoding for eGFP (see Methods). We filled a suspension of these GFP-expressing cells into a high-Q microcavity resonator formed by two highly reflective distributed Bragg reflectors (DBRs), separated by $d = 20$ μm (Fig. 2a). Figure 2b–d shows differential interference contrast (DIC) and confocal fluorescence microscopy images of a typical transfected cell. As the cell is not attached to a surface, it is rounded and has a spherical shape (diameter, ~15 μm). The intensity of green fluorescence

was relatively uniform throughout the entire cell volume. From the fluorescence intensity, we estimated the eGFP concentration in the cytoplasm to be ~300 μM. The average refractive index inside the cell is thought to be slightly larger than that of the surrounding medium[18]. The presence of a cell in the otherwise only marginally stable plane–plane resonator thus adds a refocusing element and renders the resonator stable.

Individual cells were pumped through a microscope objective with 465 nm OPO pulses. The emission from the pumped cell was observed through the same objective in an epi-detection scheme (see Methods). As in the solution-based laser, the output of a single optically pumped cell showed a distinct kink as the pump energy was increased beyond a certain level (Fig. 2e). Despite any scattering loss induced by refractive index heterogeneity within the cell, the threshold pump energy (850 ± 200 pJ) was considerably lowered compared to the solution laser and could be easily reached by a miniature pulsed or continuous-wave pump source. When pumped at energies just above the lasing threshold, the output spectrum of the cell laser consisted of a single emission peak with a narrow linewidth below the resolution of our spectrometer (FWHM < 0.04 nm), suggesting single-mode oscillation (Fig. 2f, top). As the pump energy was increased, additional emission lines with an irregular spacing appeared (Fig. 2f, bottom).

We confirmed distinct changes in output emission below and above threshold. The subthreshold spectrum contained numerous closely spaced weak peaks of similar intensity (Fig. 3a), and the emission was spatially uniform (Fig. 3b). Above the lasing threshold, a few of the spectral peaks gained in intensity (Fig. 3c), and the spatial output showed rich and irregular intensity patterns (Fig. 3d).

To understand these characteristics, we imaged the laser emission onto a modified spectrograph with its entrance slit opened widely. The diffraction grating dispersed the image in space according to its spectral components, forming a hyperspectral image of the laser output on the charge-coupled device (CCD) chip of the attached camera (Fig. 4a). Figure 4b–d compares the original emission pattern to the hyperspectral image for three lasing cells of different size. The data reveal that the seemingly random spatial patterns result from superpositions of several simultaneously active transverse laser modes. This is particularly obvious in Fig. 4b, where the bright spot at 512.98 nm (labelled [0,0]) is identified as the fundamental TEM mode. The next one (labelled [1,1], shifted by 0.44 nm) is characteristic of the first-order asymmetric mode (Fig. 1f(ii)), and even higher-order modes show up at yet shorter wavelengths. The same series of transverse modes repeats, with a 4.8 nm spacing, in a different longitudinal mode group (labelled by the mode indices $[p,m]'$).

As a focusing and waveguiding element in the resonator, the cell causes an increase in the roundtrip phase shift as the transverse mode order increases. This accounts for the observed difference in wavelength between subsequent transverse modes. For a given cell diameter of ~13.8 μm, a cavity length of 20 μm and a refractive index of the cytoplasm of ~1.365, a simple ABCD matrix model[19] predicts a transverse-mode spacing of 0.43 nm, in agreement with the 0.44 nm observed between the first two TEM modes (Supplementary Information S2). The paraxial approximation implicit to the ABCD approach is not justified for higher-order transverse modes, so the actual mode spacing gradually deviates from the prediction as the mode order increases.

We found that many of the observed transverse mode structures were neither Laguerre- nor Hermite-Gaussian, but resemble the less well-known Ince-Gaussian modes[20] (Fig. 4e–g). These modes have inherent elliptical symmetry and form the mathematically exact transition between Laguerre- and Hermite-Gaussian modes. The exact patterns and eccentricity of the modes result from the specific cell shape and the gain and refractive index profiles within the cell. We also observed that the number of concurrently lasing transverse

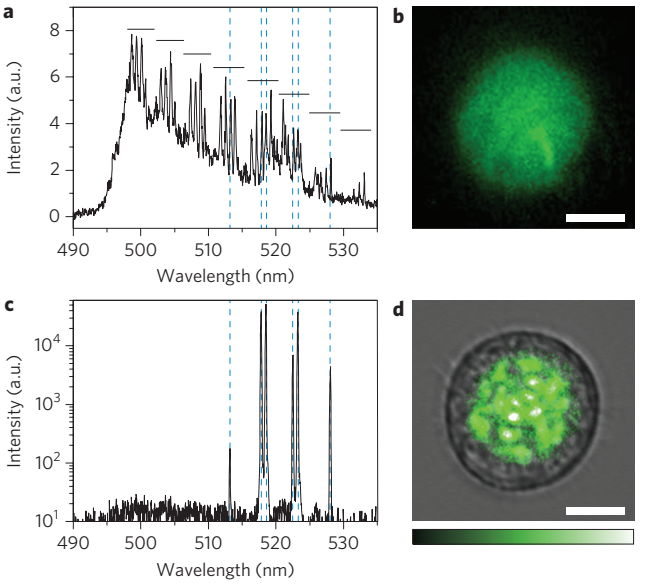

Figure 3 | Comparison of emission from the single-cell laser below and above the lasing threshold. a, Emission spectrum for the resonator pumped below the lasing threshold; the spectrum is integrated over 100 excitation pulses. Peaks located under a common horizontal black line belong to the same longitudinal mode and differ only in transverse mode order. **b**, Typical spatial patterns of the cell laser output below the lasing threshold ($E_p = 0.4$ nJ). **c**, Emission pumped 3× above lasing threshold. The spectrum is plotted on a log scale to emphasize the contrast between the laser lines and the fluorescent background. **d**, Spatial patterns of the cell laser output above threshold ($E_p = 2$ nJ) superimposed on a DIC image of the cell (black&white channel). Scale bars in **b** and **d** are 5 μm.

and longitudinal modes and their relative brightness depend on many factors, including pump energy, intracellular eGFP concentration and cell size. For each cell, the mode pattern was largely unchanged between consecutive pulses (Supplementary Fig. S3). Even at high pump energies (50 nJ/pulse, that is 50× above threshold), cells emit hundreds of laser pulses before bleaching, and we found no indication that cell viability is affected by lasing (see Methods). Cell lasing is not restricted to 293ETN cells. GFP-expressing 3T3 mouse fibroblasts also readily generated laser light.

In contrast to all previous laser materials, fluorescent proteins are biologically producible, biocompatible and bioabsorbable. They are therefore uniquely suited to generating stimulated emission and laser light from and within living organisms. The transverse mode structure is expected to be highly sensitive to the refractive index distribution in the cell and may therefore be used for three-dimensional intracellular probing[21,22]. When single-cell lasing is adapted for flow cytometry or microfluidics, the directional, bright and nanosecond pulsed emission can increase the throughput and speed of analysis, and the inherently narrowband laser emission may enable dense wavelength multiplexing. Stimulated emission is an emerging scheme to improve the resolution and sensitivity of microscopic imaging in biomedical science[23–26]. Using micro- and nanoscale resonators[27,28], it might be possible to achieve intracellular lasing without external resonators, which will enable novel nonlinear imaging schemes and allow controlled activation of photochemical therapeutic agents. Finally, the observation of lasing from single cells proves that the inherent scattering and absorption loss of biological samples can be fully compensated by stimulated emission. We expect that *in vivo* optical amplification will emerge as a general scheme to overcome the limited penetration of light in biological tissue, a factor previously considered as a fundamental limitation of optical microscopy modalities.

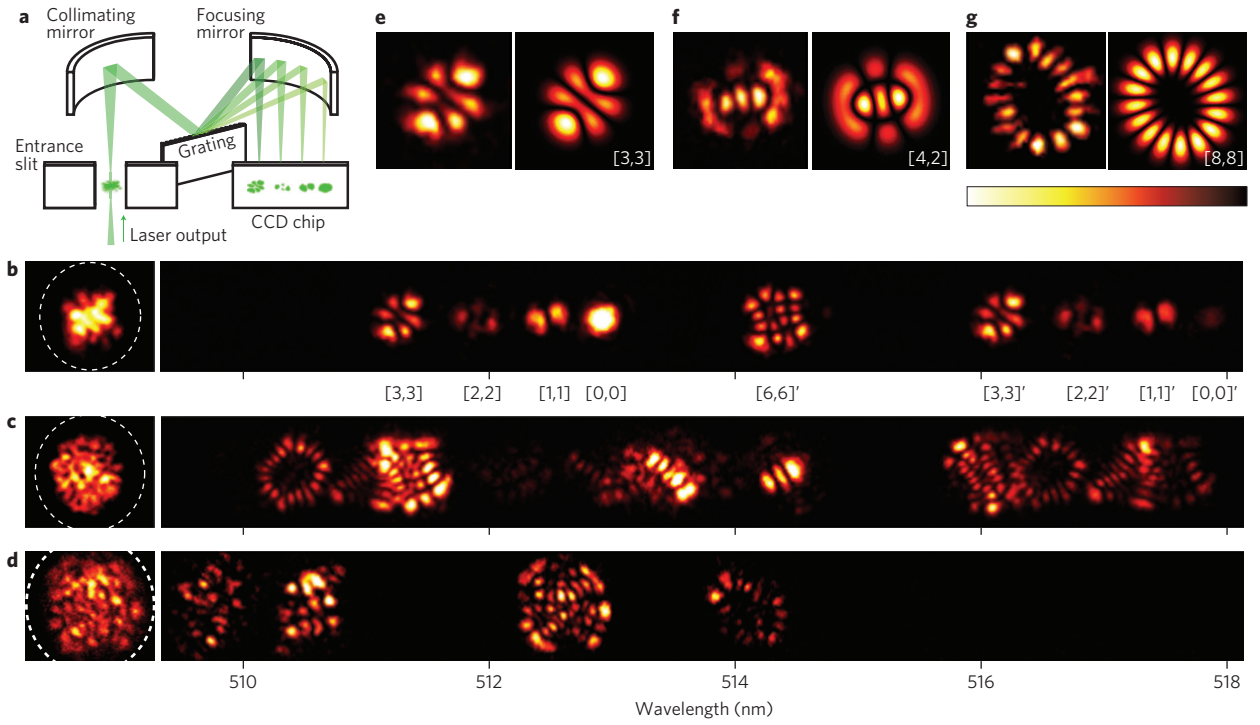

Figure 4 | Combined spatial and spectral analysis of single output pulses of different cell lasers. a, Schematic of the hyperspectral imaging setup. **b**–**d**, Single-shot analysis of the laser output. Far-field emission patterns (left part of each figure) and hyperspectral images (right part) of the concurrently lasing modes for three different 293ETN cells with diameters of 13.8 μm (**b**), 15 μm (**c**) and 17.5 μm (**d**). In **b**, the numbers denote the Ince-Gaussian mode indices [*p*,*m*]. Cells were pumped 10× above threshold. **e**–**g**, Typical measured transverse mode patterns (left part of each figure) and corresponding modelled Ince-Gaussian modes (right part, ellipticity parameter $\varepsilon = 2$). **e** corresponds to the cell shown in **b**. **f** and **g** are different cells.

Methods

Solution-based lasers. The laser cavity was formed by two highly reflective laser mirrors (Y2 coating, CVI). The optical axis of the cavity was normal to the surface of the optical table. A recombinant eGFP solution (400 μl) of defined concentration was deposited on the reflective surface of the lower of the two mirrors (radius of curvature, $r_1 = 10$ mm) and the mirrors were caused to approach towards one another until the solution was in contact with the upper mirror ($r_2 = 50$ mm). The mirrors were then slowly separated to a distance of 7 mm. The eGFP solution maintained contact with the hydrophilic surface of both mirrors, eliminating any surface reflection loss inside the cavity.

The energy of the pulses emitted by the OPO (Quanta Ray MOPO-700, Spectra Physics; pulse duration, ~5 ns, tuned to 465 nm) was adjusted with neutral density filters and monitored with an energy meter. The pulses were reflected into the laser cavity described above by a dichroic mirror (500 nm, long-pass) and focused with a 30 mm lens. The pulse energies quoted in this paper represent the energy of single pulses behind the focusing lens. The focus of the beam was located close to the surface of the upper mirror to best match the profile of the excitation beam with the profile of the fundamental cavity mode across the cavity. The emission from the cavity was collected through the same 30 mm lens, separated from back-reflected excitation light by the dichroic mirror and split with a 50/50 beamsplitter. One part of the signal was then imaged by a camera; the other part was fibre-coupled to a 300 mm spectrograph connected to a cooled CCD camera (Andor). See Fig. 1b for a schematic illustration of the setup.

Single-cell lasers. 293ETN cells were grown in complete growth medium under standard incubation conditions (37 °C, 5% CO_2) until about 50% confluent. Cells were transfected with a peak15 plasmid encoding for eGFP under control of the Chicken Beta actin promoter with a CMV enhancer using GeneJuice (Novagen) as transfection reagent. The cells were harvested with trypsin at 72 h post-transfection and selected for green fluorescence using standard fluorescence assisted cell sorting (FACS ARIA III, BD). Cells were washed and resuspended in fresh culture medium to a density of ~500,000 cells ml^{-1}.

The laser resonator was formed by gluing together two quartz substrates coated with highly reflective DBRs, with glass spacer beads of calibrated diameter as spacers. When a droplet of the cell suspension (~10 μl) was placed onto the edge of the mirror pair, the capillary force rapidly pulled the cells into the resonator. The concentration of the cell suspension was such that the cells did not coagulate and on average were spaced by at least 100 μm when inside the resonator. The cells were kept in their usual culture medium for the entire experiment to ensure optimum cell viability.

The cells were optically pumped using a similar setup as described above, but the 30 mm lens was replaced by a 40× objective so that cells could be imaged. The resonator was mounted on an *xyz*-micropositioning stage to position individual cells in the centre of the pump beam. The pump beam was made slightly divergent before it entered the objective by inserting an additional lens into the optical path. This arrangement shifted the beam focus away from the imaging plane of the objective lens and ensured that the entire cell volume was homogeneously excited by the pump laser.

To record hyperspectral images, the fibre coupling to the spectrograph was removed and the output of the cell laser was imaged directly onto the entrance slit of the spectrograph. In this way the spatial pattern associated with each emission line was projected onto a different location on the CCD chip of the camera attached to the spectrograph. The entrance slit was opened wide enough to collect the entire laser output pattern. The spectrograph was equipped with a holographic 2,400 lines mm^{-1} grating to achieve maximum dispersion of the signal. The hyperspectral images shown in this paper were obtained with single output pulses of the cell laser.

To check if the lasing process harmed the cells, we supplemented the cell dispersion with ethidium homodimer-1 (EthD-1). EthD-1 is normally excluded from the inside of live cells but readily passes through the membrane of dead cells. On binding to intracellular nucleic acids, the normally weakly fluorescent material generates bright red fluorescence. In our experiment, the lasing process did not result in a measurable increase of red fluorescence from the corresponding cells, even after prolonged exposure to high pump energies (1,000 pulses, 50 nJ/pulse, that is, 50× above threshold). When the pump energy was increased even further (beyond 1 μJ/pulse) the cells were physically damaged and the characteristic EthD-1 fluorescence was observed.

Received 4 January 2011; accepted 13 April 2011; published online 12 June 2011

References

1. Maiman, T. H. Stimulated optical radiation in ruby. *Nature* **187,** 493–494 (1960).
2. Weber, M. J. *Handbook of Laser Wavelengths* (CRC Press, 1999).
3. Townes, C. H. *How the Laser Happened: Adventures of a Scientist* (Oxford Univ. Press, 1999).
4. Shaner, N. C., Steinbach, P. A. & Tsien, R. Y. A guide to choosing fluorescent proteins. *Nature Methods* **2,** 905–909 (2005).
5. Giepmans, B. N. G., Adams, S. R., Ellisman, M. H. & Tsien, R. Y. Review—the fluorescent toolbox for assessing protein location and function. *Science* **312,** 217–224 (2006).

6. Shimomura, O., Johnson, F. H. & Saiga, Y. Extraction, purification and properties of aequorin, a bioluminescent protein from luminous hydromedusan, *Aequorea*. *J. Cell. Comp. Physiol.* **59,** 223–239 (1962).
7. Chalfie, M., Tu, Y., Euskirchen, G., Ward, W. W. & Prasher, D. C. Green fluorescent protein as a marker for gene-expression. *Science* **263,** 802–805 (1994).
8. Heim, R., Cubitt, A. B. & Tsien, R. Y. Improved green fluorescence. *Nature* **373,** 663–664 (1995).
9. Cormack, B. P., Valdivia, R. H. & Falkow, S. Facs-optimized mutants of the green fluorescent protein (gfp). *Gene* **173,** 33–38 (1996).
10. Shaner, N. C. *et al.* Improved monomeric red, orange and yellow fluorescent proteins derived from *Discosoma* sp. red fluorescent protein. *Nature Biotechnol.* **22,** 1567–1572 (2004).
11. Merzlyak, E. M. *et al.* Bright monomeric red fluorescent protein with an extended fluorescence lifetime. *Nature Methods* **4,** 555–557 (2007).
12. Patterson, G. H., Knobel, S. M., Sharif, W. D., Kain, S. R. & Piston, D. W. Use of the green fluorescent protein and its mutants in quantitative fluorescence microscopy. *Biophys. J.* **73,** 2782–2790 (1997).
13. Pikas, D. J. *et al.* Nonlinear saturation and lasing characteristics of green fluorescent protein. *J. Phys. Chem. B* **106,** 4831–4837 (2002).
14. Siegman, A. E. *Lasers* (University Science Books, 1986).
15. Chen, Y., Wei, L. N. & Muller, J. D. Probing protein oligomerization in living cells with fluorescence fluctuation spectroscopy. *Proc. Natl Acad. Sci. USA* **100,** 15492–15497 (2003).
16. Lu, P., Vogel, C., Wang, R., Yao, X. & Marcotte, E. M. Absolute protein expression profiling estimates the relative contributions of transcriptional and translational regulation. *Nature Biotechnol.* **25,** 117–124 (2007).
17. Kim, H. & Seed, B. The transcription factor MafB antagonizes antiviral responses by blocking recruitment of coactivators to the transcription factor IRF3. *Nature Immunol.* **11,** 743–750 (2010).
18. Kemper, B. *et al.* Integral refractive index determination of living suspension cells by multifocus digital holographic phase contrast microscopy. *J. Biomed. Opt.* **12,** 054009 (2007).
19. Svelto, O. *Principles of Lasers* (Springer-Verlag, 2009).
20. Bandres, M. A. & Gutiérrez-Vega, J. C. Ince-Gaussian modes of the paraxial wave equation and stable resonators. *J. Opt. Soc. Am. A* **21,** 873–880 (2004).
21. Rose, A., Zhu, Z. G., Madigan, C. F., Swager, T. M. & Bulovic, V. Sensitivity gains in chemosensing by lasing action in organic polymers. *Nature* **434,** 876–879 (2005).
22. Park, Y. *et al.* Refractive index maps and membrane dynamics of human red blood cells parasitized by *Plasmodium falciparum*. *Proc. Natl Acad. Sci. USA* **105,** 13730–13735 (2008).
23. Klar, T. A., Jakobs, S., Dyba, M., Egner, A. & Hell, S. W. Fluorescence microscopy with diffraction resolution barrier broken by stimulated emission. *Proc. Natl Acad. Sci. USA* **97,** 8206–8210 (2000).
24. Westphal, V. *et al.* Video-rate far-field optical nanoscopy dissects synaptic vesicle movement. *Science* **320,** 246–249 (2008).
25. Min, W. *et al.* Imaging chromophores with undetectable fluorescence by stimulated emission microscopy. *Nature* **461,** 1105–1109 (2009).
26. Saar, B. G. *et al.* Video-rate molecular imaging *in vivo* with stimulated Raman scattering. *Science* **330,** 1368–1370 (2010).
27. Noginov, M. A. *et al.* Demonstration of a spaser-based nanolaser. *Nature* **460,** 1110–1113 (2009).
28. Ma, R.-M., Oulton, R. F., Sorger, V. J., Bartal, G. & Zhang, X. Room-temperature sub-diffraction-limited plasmon laser by total internal reflection. *Nature Mater.* **10,** 110–113 (2011).

Acknowledgements

The authors thank Ji-Joon Song (KAIST, Korea) for providing recombinant eGFP solutions, S. Sassi and B. Seed (Harvard Medical School) for the donation of 293ETN cells and support with eGFP transfection, U. Shama for initial testing of a fluorescent protein and W. Farinelli for setting up the OPO system. This work was supported in part by the US National Science Foundation (ECCS-1101947) and the Korea National Research Foundation (R31-2008-000-10071-0). M.C.G. acknowledges financial support from the Bullock-Wellman Fellowship.

Author contributions

M.C.G. designed and performed the experiments. S.H.Y conceived and supervised the project. Both authors discussed the data and wrote the paper.

Additional information

The authors declare no competing financial interests. Supplementary information accompanies this paper at www.nature.com/naturephotonics. Reprints and permission information is available online at http://www.nature.com/reprints/. Correspondence and requests for materials should be addressed to S.H.Y.